

This is the accepted manuscript made available via CHORUS. The article has been published as:

Generalized Landau level representation: Effect of static screening in the quantum Hall effect in graphene

Igor A. Shovkovy and Lifang Xia

Phys. Rev. B **93**, 035454 — Published 28 January 2016

DOI: [10.1103/PhysRevB.93.035454](https://doi.org/10.1103/PhysRevB.93.035454)

Generalized Landau-level representation: effect of static screening in quantum Hall effect in graphene

Igor A. Shovkovy^{1,*} and Lifang Xia^{2,†}

¹*College of Letters and Sciences, Arizona State University, Mesa, Arizona 85212, USA*

²*Department of Physics, Arizona State University, Tempe, Arizona 85287, USA*

By making use of the generalized Landau-level representation (GLLR) for the quasiparticle propagator, we study the effect of screening on the properties of the quantum Hall states with integer filling factors in graphene. The analysis is performed in the low-energy Dirac model in the mean-field approximation, in which the long-range Coulomb interaction is modified by the one-loop static screening effects in the presence of a background magnetic field. By utilizing a rather general ansatz for the propagator, in which all dynamical parameters are running functions of the Landau-level index n , we derive a self-consistent set of the Schwinger-Dyson (gap) equations and solve them numerically. The explicit solutions demonstrate that static screening leads to a substantial suppression of the gap parameters in the quantum Hall states with a broken $U(4)$ flavor symmetry. The temperature dependence of the energy gaps is also studied. The corresponding results mimic well the temperature dependence of the activation energies measured in experiment. It is also argued that, in principle, the Landau-level running of the quasiparticle dynamical parameters could be measured via optical studies of the integer quantum Hall states.

PACS numbers: 73.22.Pr, 71.70.Di, 71.70.-d

I. INTRODUCTION

As predicted theoretically more than three decades ago^{1,2}, the low-energy excitations in planar graphite, or graphene are described by $(2+1)$ -dimensional, massless Dirac fermions. Interestingly, the spinor structure of the corresponding fermion fields has nothing to do with the usual spin of electrons. It is connected with an effective “pseudospin” that has its roots in the hexagonal arrangement of carbon atoms in graphene, which can be viewed as a superposition of two inequivalent triangular sublattices. At the same time, the usual spin plays a rather passive role analogous to an extra “species” degree of freedom.

The Dirac nature of excitations was confirmed experimentally by the observation of the anomalous integer quantum Hall (QH) effect in Refs.^{3,4}. At sufficiently low temperatures, the measured Hall conductivity revealed a set of well-resolved QH plateaus at the filling factors $\nu = \pm 4(k + 1/2)$, where $k = 0, 1, 2, \dots$ is an integer. One of the signature properties of the corresponding QH effect is the anomalous shift of $1/2$ in the expression for the filling factor. This measurement appears to be in perfect agreement with the theoretical predictions of the low-energy Dirac theory⁵⁻⁸. The overall factor of 4 in the expression for ν is also in agreement with the predicted fourfold (spin and sublattice-valley) degeneracy of the Landau levels in the low-energy theory. For reviews of quantum Hall physics in graphene see Ref.⁹⁻¹¹.

The spin and sublattice-valley degeneracy of the Landau levels in the low-energy theory of graphene can be associated with an approximate global “flavor” $U(4)$ symmetry. Strictly speaking, the symmetry is not exact. There exist several small explicit symmetry breaking effects that lift the degeneracy of the Landau levels¹². The most obvious among them is the Zeeman effect that breaks the $U(4)$ symmetry down to $U_\uparrow(2) \times U_\downarrow(2)$, where $U_s(2)$ with $s = \uparrow, \downarrow$ is the sublattice-valley symmetry of quasiparticles with a fixed spin. In practice, however, the flavor $U(4)$ symmetry could be treated as exact because, for any realistic value of the magnetic field, the Zeeman energy is much smaller than the Landau energy scale. Moreover, the Zeeman energy, as well as all other explicit symmetry breaking effects are negligible not only compared to the Landau energy scale, but even compared to the nonzero (thermal/interaction) widths of the individual Landau levels. This explains why it is hard to resolve experimentally the QH plateaus with any filling factors other than $\nu = \pm 4(k + 1/2)$ that correspond to fully filled fourfold-degenerate Landau levels.

The subsequent experimental studies revealed that, in sufficiently strong magnetic fields, additional QH plateaus at $\nu = 0, \pm 1, \pm 3, \pm 4$ can be resolved¹³⁻²⁵. As is clear, the corresponding QH states have fractional fillings of the low-lying Landau levels. The implication of this is that the approximate fourfold degeneracy of the Landau levels is truly lifted. Such new QH states could be explained theoretically if the electron-electron interaction triggers spontaneous breaking of the flavor $U(4)$ symmetry. For example, the symmetry breaking $U(4) \rightarrow U_\uparrow(2) \times U_\downarrow(2)$ by a *dynamically enhanced* Zeeman splitting could potentially explain the origin of the QH states with $\nu = 0$ and $\nu = \pm 4$. If realized, such a scenario would be nothing else, but a textbook example of the QH ferromagnetism (QHF)²⁶⁻³¹ [see also Ref.³²].

It should be emphasized, however, that QHF is not the only possibility. There exist a number of symmetry breaking mechanisms and residual symmetries consistent with the filling factors of the additional QH states. One of such alter-

native scenarios utilizes the idea of magnetic catalysis (MC)^{33–35}. The corresponding order parameters are excitonic (particle-hole) condensates responsible for the generation of the Dirac and/or Haldane masses of quasiparticles^{6,36–43}. At the microscopic level, the excitonic condensates corresponds to a charge density wave (CDW), or a valley polarized CDW. Symmetry arguments, as well as direct effective model studies^{40,41} suggest that the order parameters associated with the MC and QHF scenarios necessarily coexist. Also, in principle, these two could reproduce all integer QH plateaus observed experimentally in strong magnetic fields. With that being said, a number of different types of order parameters are possible^{42–47}. It is also fair to note that the precise nature of the observed integer QH states is not always unambiguous from theoretical considerations and not always established unambiguously in experiment.

From the experimental point of view, a lot of effort was devoted to revealing the underlying nature of the strongly insulating $\nu = 0$ QH state, associated with half-filling of the lowest Landau level^{13–25}. The main advances in resolving the nature of the QH states were made by applying a tilted magnetic field to high-quality graphene devices, that were fabricated on a thin hexagonal boron nitride substrate^{23,24} or encapsulated between two layers of hexagonal boron nitride²⁵. In the case of $\nu = 0$ QH state, in particular, a careful analysis of the conductance and the bulk density of states^{23–25} suggests that the state is not spin polarized when the magnetic field is perpendicular to the plane of graphene. This is consistent, for example, with both an antiferromagnet and a charge density wave. When an in-plane component of the magnetic field increases, the state gradually transforms into a fully polarized ferromagnetic state. In the intermediate regime, a canted antiferromagnetic state is presumably realized⁴⁴. Such an interpretation is supported by the observation of the bulk gap that does not close and the edge states that become conducting with increasing of the total magnetic field. Considering, however, how heavily the arguments rely on the properties of the edge states, the final conclusions should be still accepted with a caution.

The high-quality graphene devices in Refs.^{23,25} also reveal a large sequence of integer QH states with $\nu \geq 1$. Among these, there are two states associated with quarter filling of the lowest Landau level, i.e., $\nu = \pm 1$. The linear growth of the energy gaps in these two states as a function of the total magnetic field points to their spin polarized nature and the major role played by the Zeeman energy in aligning the ground state. A similar sensitivity to the Zeeman energy is also observed for the states associated with half-filling of higher Landau levels, i.e., $\nu = 4n$, but not for the states with quarter and three-quarter fillings, i.e., $\nu = 4n \pm 1$ ²³. As we will see, most of these features are reproduced in the model studied here.

In the mean-field approximation, the role of the long-range Coulomb interaction and Landau-level mixing were studied in Ref.⁴⁸. By utilizing a rather general combination of the MC and QHF order parameters, the corresponding study was able to reproduce all observed QH plateaus (i.e., $\nu = 0, \pm 1, \pm 3, \pm 4$) as well as to suggest that QH plateaus with any integer filling are possible. The symmetry breaking patterns of the solutions obtained in the model with the long-range Coulomb interaction appeared to be similar to those in the model with local four-fermion interaction in Ref.⁴¹. The qualitative effects due to the long-range force were (i) Landau-level mixing and (ii) “running” of all dynamical parameters (i.e., the wavefunction renormalization parameters, the Dirac and Haldane masses) as functions of the Landau-level index.

In this paper, we extend the study of the abnormal integer QH effect in the model with the long-range Coulomb interaction⁴⁸ by including the screening effects and the effects of nonzero temperature. By making use of a similar mean-field approximation that neglects the fluctuations of order parameters, we will derive the full quasiparticle propagators in the GLLR formalism for all qualitatively different series of QH states with integer filling factors. (A semi-rigorous justification of the approximation used will be provided in Sec. II C.) As expected, the corresponding results contain not only the information about the energy gaps at the Fermi level, but also the complete dispersion relations of quasiparticles in all Landau levels. The resulting propagators can be used in transport calculations, predictions of various emission and absorption rates, etc.

This paper is organized as follows. In Sec. II, we briefly introduce the model, define the quasiparticle propagator, and derive the gap equations. In Sec. III, we present our numerical analysis of the gap equations and classify the main types of solutions. We also compare our results with those in the previous studies. The summary of the main results is given in Sec. IV.

II. THE MODEL

Following the same approach as in Ref.⁴⁸, in this study we will use the language of the low-energy theory for the description of the QH effect in monolayer graphene. The low-energy quasiparticle fields are given by the following four-component Dirac spinors $\Psi_s = (\psi_{KAs}, \psi_{KBs}, \psi_{K'Bs}, -\psi_{K'As})$, which combine the Bloch states on the two different sublattices (A, B) of the hexagonal graphene lattice in coordinate space. The components labeled by the valley indices K and K' correspond to the Bloch states with the momenta from the vicinity of the corresponding inequivalent Dirac points (K or K') in the two-dimensional Brillouin zone. The field Ψ_s also carries an additional index that describes the spin state, i.e., $s = \uparrow, \downarrow$.

A. Quasiparticle Hamiltonian

The free quasiparticle Hamiltonian has the following pseudorelativistic form:

$$H_0 = v_F \int d^2\mathbf{r} \bar{\Psi} (\gamma^1 \pi_x + \gamma^2 \pi_y) \Psi, \quad (1)$$

where $v_F \approx 10^6 \text{ m/s}$ is the Fermi velocity, $\mathbf{r} = (x, y)$ is the position vector in the plane of graphene, and $\bar{\Psi} = \Psi^\dagger \gamma^0$ is the Dirac-conjugated spinor. Note that the sum over the spin states is implicit in Eq. (1). The canonical momentum $\boldsymbol{\pi} = -i\hbar - e\mathbf{A}/c$ includes the vector potential \mathbf{A} that corresponds to the magnetic field component \mathbf{B}_\perp orthogonal to the plane of graphene. The 4×4 Dirac matrices γ^ν (with $\nu = 0, 1, 2$) are defined as follows: $\gamma^\nu = \tilde{\tau}^3 \otimes (\tau^3, i\tau^2, -i\tau^1)$, where the two sets of Pauli matrices $\tilde{\tau}$ and τ act in the valley (K, K') and sublattice (A, B) spaces, respectively. They satisfy the usual anticommutation relations $\{\gamma^\mu, \gamma^\nu\} = 2g^{\mu\nu}$, where $g^{\mu\nu} = \text{diag}(1, -1, -1)$, and $\mu, \nu = 0, 1, 2$.

In order to be able to describe QH states with arbitrary filling factors, we should also allow for a nonzero electron chemical potential μ_e . The latter is introduced via an additional term, $-\mu_e \int d^2\mathbf{r} \Psi^\dagger \Psi$, in the free Hamiltonian in Eq. (1). The long range Coulomb interaction is included in the low-energy Hamiltonian by adding the following term:

$$H_C = \frac{1}{2} \int d^2\mathbf{r} d^2\mathbf{r}' \Psi^\dagger(\mathbf{r}) \Psi(\mathbf{r}) U_C(\mathbf{r} - \mathbf{r}') \Psi^\dagger(\mathbf{r}') \Psi(\mathbf{r}'), \quad (2)$$

where $U_C(\mathbf{r} - \mathbf{r}')$ is the coordinate-space Coulomb potential in the presence of a constant magnetic field. It is straightforward to check that the resulting Hamiltonian $H = H_0 + H_C - \mu_e \int d^2\mathbf{r} \Psi^\dagger \Psi$ is invariant under the flavor $U(4)$ symmetry that combines the transformations in spin and sublattice-valley spaces. For the explicit form of the symmetry generators see, for example, Ref.⁶. Such a flavor symmetry is explicitly (although weakly) broken by the Zeeman interaction of the quasiparticle spin with the external magnetic field \mathbf{B} . The additional interaction term in the Hamiltonian is given by $\int d^2\mathbf{r} \mu_B B \Psi^\dagger \sigma^3 \Psi$, where $B = |\mathbf{B}|$, $\mu_B = e\hbar/(2mc)$ is the Bohr magneton, and σ^3 is the Pauli matrix acting in the spin space. As is easy to check, the Zeeman term breaks the $U(4)$ symmetry down to the $U_\uparrow(2) \times U_\downarrow(2)$ symmetry.

The complete model Hamiltonian, including the Zeeman interaction and the electron chemical potential μ_e , can be conveniently rewritten in the following quasirelativistic form:

$$H = \int d^2\mathbf{r} \bar{\Psi} [v_F(\boldsymbol{\pi} \cdot \boldsymbol{\gamma}) - \mu_e \gamma^0 + \mu_B B \sigma^3 \gamma^0] \Psi + H_C. \quad (3)$$

This implies that the inverse bare quasiparticle propagator is defined by the following expression:

$$iS^{-1}(\omega; \mathbf{r}, \mathbf{r}') = [(\omega + \mu_e - \mu_B B \sigma^3) \gamma^0 - v_F(\boldsymbol{\pi} \cdot \boldsymbol{\gamma})] \delta(\mathbf{r} - \mathbf{r}'). \quad (4)$$

Here and below, it is convenient to use a mixed (ω, \mathbf{r}) -representation.

Let us note in passing that a certain degree of disorder is always present in real graphene devices and, in fact, plays a critical role in the observation of the quantum Hall plateaus. However, in the model analysis below, which concentrates primarily on the delocalized quasiparticles states in the bulk of graphene, it is justifiable to ignore disorder. Indeed, when the spectrum of the delocalized states is established, a large number of bulk observables (e.g., symmetry properties of the QH states, density of states, energy of transitions lines, activation energies, etc.) will be predicted without much ambiguity. The corresponding limitation is not so critical also because of the robustness of the QH effect that stem from its topological nature.

B. Dynamical symmetry breaking and full quasiparticle propagator

In order to be able to describe various QH states with integer fillings factors, we use a rather general ansatz for the full quasiparticle propagator⁴⁸,

$$G^{-1}(\omega; \mathbf{r}, \mathbf{r}') = -i \left[(\gamma^0 \omega - v_F \hat{F}^+ (\boldsymbol{\pi} \cdot \boldsymbol{\gamma}) + \hat{\Sigma}^+) \right] \delta(\mathbf{r} - \mathbf{r}'), \quad (5)$$

where \hat{F}^+ and $\hat{\Sigma}^+$ are operator-valued wavefunction renormalization and self-energy functions, respectively. For simplicity, here we will assume that the propagator is a diagonal 2×2 matrix in the spinor space, or in other words that the propagator for *each* of the two spin states looks like that in Eq. (5). As is clear, such a choice of the ansatz for the propagator does not allow spin mixing. As a result, one cannot describe certain types of states (e.g., a canted

antiferromagnetism⁴⁴). Nevertheless, we emphasize that the ansatz in Eq. (5) is extremely flexible and can describe a large number of states (with very different symmetry properties) for each integer filling factor. In the case of filling factor $\nu = 0$, for example, these include a charge/spin density waves, as well as ferromagnetic and antiferromagnetic states. The latter are basically all main options proposed for a configuration with a magnetic field perpendicular to the plane of graphene.

By construction, both \hat{F}^+ and $\hat{\Sigma}^+$ are functions of the three mutually commuting dimensionless operators: γ^0 , $is_\perp\gamma^1\gamma^2$, and $(\boldsymbol{\pi} \cdot \boldsymbol{\gamma})^2 l^2$, where $s_\perp = \text{sign}(eB)$ and $l = \sqrt{\hbar c/|eB_\perp|}$ is the magnetic length. In principle, they could also depend on the quasiparticle energy ω . Taking into account that $(\gamma^0)^2 = \mathbb{I}$ and $(is_\perp\gamma^1\gamma^2)^2 = \mathbb{I}$, the Dirac structure of the operator-valued functions \hat{F}^+ and $\hat{\Sigma}^+$ can be written in the following form:

$$\hat{F}^+ = f + \gamma^0 g + is_\perp\gamma^1\gamma^2\tilde{g} + is_\perp\gamma^0\gamma^1\gamma^2\tilde{f}, \quad (6)$$

$$\hat{\Sigma}^+ = \tilde{\Delta} + \gamma^0\mu + is_\perp\gamma^1\gamma^2\tilde{\mu} + is_\perp\gamma^0\gamma^1\gamma^2\Delta, \quad (7)$$

where $f, \tilde{f}, g, \tilde{g}, \tilde{\Delta}, \Delta, \mu$, and $\tilde{\mu}$ are functions of only one operator, $(\boldsymbol{\pi} \cdot \boldsymbol{\gamma})^2 l^2$. To a large degree the physical meaning of the corresponding operators should be clear from their Dirac structure and symmetry properties. In particular, the eigenvalues of the first four of them (f, \tilde{f}, g , and \tilde{g}) will play the role of generalized wavefunction renormalizations, while the others will be playing the role of the generalized the MC and QHF order parameters, i.e., the Dirac (parity-even) and Haldane (parity-odd) masses (i.e., Δ and $\tilde{\Delta}$) and chemical potentials (i.e., μ and $\tilde{\mu}$). As will see, such an interpretation is also supported by the role of the corresponding parameters in the dispersion relations of quasiparticles, see Eqs. (13) and (14) below.

The three mutually commuting operators, γ^0 , $is_\perp\gamma^1\gamma^2$, and $(\boldsymbol{\pi} \cdot \boldsymbol{\gamma})^2 l^2$, allow a common basis of eigenstates, $|s_0, s_{12}, n\rangle$. The corresponding eigenvalues are $s_0 = \pm 1$, $s_{12} = \pm 1$, and $-2n = -(2N + 1 + s_\perp s_{12})$, respectively, where $N = 0, 1, 2, \dots$ is the quantum number of the orbital angular momentum and s_{12} is the sign of the pseudospin projection. By making use of the complete set of eigenstates $|s_0, s_{12}, n\rangle$, one can derive a very convenient generalized Landau-level representation (GLLR) of the (inverse) quasiparticle propagator (5). (For details of the derivation, see Appendix A in Ref.⁴⁸.) The final form of the *inverse* full propagator is given by

$$G^{-1}(\omega; \mathbf{r}, \mathbf{r}') = e^{i\Phi(\mathbf{r}, \mathbf{r}')} \tilde{G}^{-1}(\omega; \mathbf{r} - \mathbf{r}'), \quad (8)$$

where $\Phi(\mathbf{r}, \mathbf{r}') = -s_\perp \frac{(x+x')(y-y')}{2l^2}$ is the well-known Schwinger phase in an external magnetic field in the Landau gauge $\mathbf{A} = (0, Bx)$. The translation invariant part of the inverse GLLR propagator is given by

$$\begin{aligned} \tilde{G}^{-1}(\omega; \mathbf{r}) = & -i \frac{e^{-\xi/2}}{2\pi l^2} \sum_{n=0}^{\infty} \sum_{s_0=\pm 1} \sum_{\sigma=\pm 1} \left\{ s_0 \omega L_n(\xi) + (s_0 \mu_{n,\sigma} + \tilde{\Delta}_{n,\sigma}) [\delta_{-\sigma}^{s_0} L_n(\xi) + \delta_{+\sigma}^{s_0} L_{n-1}(\xi)] \right. \\ & \left. + i \frac{v_F^2}{l^2} (\boldsymbol{\gamma} \cdot \mathbf{r}) (f_{n,\sigma} - s_0 g_{n,\sigma}) L_{n-1}^1(\xi) \right\} \mathcal{P}_{s_0, s_0 \sigma}, \end{aligned} \quad (9)$$

where $\xi = \mathbf{r}^2/(2l^2)$ and L_n^α are the Laguerre polynomials. (Here, by definition, $L_n^0 \equiv L_n$ and $L_{n<0}^\alpha = 0$.) In Eq. (9), we also used the following set of eigenstate projectors in the Dirac space: $P_{s_0, s_{12}} = \frac{1}{4}(1 + s_0 \gamma^0)(1 + s_{12} is_\perp \gamma^1 \gamma^2)$, as well as the following shorthand notations for the linear combinations of the order parameters:

$$\mu_{n,\sigma} = \mu_n + \sigma \tilde{\mu}_n, \quad \tilde{\Delta}_{n,\sigma} = \tilde{\Delta}_n + \sigma \Delta_n, \quad f_{n,\sigma} = f_n + \sigma \tilde{f}_n, \quad g_{n,\sigma} = g_n + \sigma \tilde{g}_n, \quad (10)$$

where $\sigma \equiv s_0 s_{12}$. Note that the parameters $f_n, \tilde{f}_n, g_n, \tilde{g}_n, \tilde{\Delta}_n, \Delta_n, \mu_n$, and $\tilde{\mu}_n$ are associated with the n th Landau level. They are obtained by calculating the eigenvalues of the corresponding operators, introduced on the right-hand side of Eqs. (6) and (7).

Similarly, the full GLLR propagator takes the form⁴⁸

$$G(\omega; \mathbf{r}, \mathbf{r}') = e^{i\Phi(\mathbf{r}, \mathbf{r}')} \tilde{G}(\omega; \mathbf{r} - \mathbf{r}'), \quad (11)$$

where the Schwinger phase is exactly the same as in Eq. (8) and the translation invariant part of the propagator reads

$$\begin{aligned} \tilde{G}(\omega; \mathbf{r}) = & i \frac{e^{-\xi/2}}{2\pi l^2} \sum_{n=0}^{\infty} \sum_{s_0=\pm 1} \sum_{\sigma=\pm 1} \left\{ \frac{s_0(\omega + \mu_{n,\sigma}) + \tilde{\Delta}_{n,\sigma}}{(\omega + \mu_{n,\sigma})^2 - E_{n,\sigma}^2} [\delta_{-\sigma}^{s_0} L_n(\xi) + \delta_{+\sigma}^{s_0} L_{n-1}(\xi)] \right. \\ & \left. + i \frac{v_F^2}{l^2} (\boldsymbol{\gamma} \cdot \mathbf{r}) \frac{f_{n,\sigma} - s_0 g_{n,\sigma}}{(\omega + \mu_{n,\sigma})^2 - E_{n,\sigma}^2} L_{n-1}^1(\xi) \right\} \mathcal{P}_{s_0, s_0 \sigma}, \end{aligned} \quad (12)$$

The explicit form of the Landau level energies $E_{n,\sigma}$ are given by

$$E_{0,\sigma} = \sigma \tilde{\Delta}_{0,\sigma} = \Delta_0 + \sigma \tilde{\Delta}_0, \quad (13)$$

$$E_{n,\sigma} = \sqrt{2n(f_{n,\sigma}^2 - g_{n,\sigma}^2)v_F^2/l^2 + \tilde{\Delta}_{n,\sigma}^2}, \quad n \geq 1. \quad (14)$$

The corresponding quasiparticles energies are determined by the location of the poles of the propagator (12), namely $\omega_{0,\sigma} = -\mu_{0,\sigma} + E_{0,\sigma}$ and $\omega_{n,\sigma}^\pm = -\mu_{n,\sigma} \pm E_{n,\sigma}$ for $n \geq 1$.

Note that the expressions for the Landau level energies in Eqs. (13) and (14) shed additional light on the physical meaning of the various dynamical parameters, used in the ansatz of the full quasiparticle propagator. In particular, as we can see, the combination of the wavefunction renormalization parameters $\sqrt{f_{n,\sigma}^2 - g_{n,\sigma}^2}$ determines the renormalization of the quasiparticle velocity parameter. Also, we see that the absolute value of $\tilde{\Delta}_{n,\sigma}$ plays the role of a mass.

C. Schwinger-Dyson (gap) equation with static screening

In order to derive the GLLR form of the Schwinger-Dyson (gap) equation, we will start from the standard coordinate form of the gap equation in the random-phase approximation (RPA) and assume that the interaction is provided by the long-range Coulomb force subject to static screening effects. Such a consideration will amend the analysis of Ref.⁴⁸, where the corresponding gap equation was analyzed in the approximation without screening. Our goal here is to illuminate the qualitative and quantitative role played by screening.

It is important to emphasize that we will use a mean-field method that ignores the fluctuations of order parameters. While this is a common approximation used in numerous theoretical studies, there is no rigorous justification of its validity. Formally, the corresponding fluctuations can destroy any long-range order in 2D when $T \neq 0$ and, thus, prevent any spontaneous breakdown of continuous symmetries. We argue semi-rigorously that this may not be the case for finite-size, high-quality graphene devices fabricated on substrates. The substrate could make certain aspects of dynamics in graphene effectively three-dimensional and, thus, tame the dangerous fluctuations (at least on the length scales of typical devices) that would destroy the long-range order in an ideal 2D graphene. Admittedly, however, this issue requires a more careful investigation in the future studies.

After taking into account the condition of overall charge neutrality in graphene, we arrive at the following gap equation for the translation invariant part of the quasiparticle propagator⁴⁸:

$$\tilde{G}^{-1}(\omega; \mathbf{r}) = \tilde{S}^{-1}(\omega; \mathbf{r}) + e^2 \gamma^0 \tilde{G}(\omega; \mathbf{r}) \gamma^0 D(\omega; \mathbf{r}), \quad (15)$$

where $D(\omega; \mathbf{r})$ is the time-like component of the gauge (photon) field propagator that contains all the information about the interaction. As stated before, we will use an approximation with Coulomb interaction that includes the effects of static screening. In essence, this is the instantaneous approximation⁶ that neglects the retardation of the interaction. One might argue that this is a reasonable approximation because charge carriers are much slower than the speed of light. (See, however, Refs.^{49,50} suggesting that dynamical screening could affect the dynamics quantitatively.) Therefore, we use an energy independent polarization function, i.e., $\Pi(\omega, \mathbf{k}) \simeq \Pi(0, \mathbf{k})$, in order to model the effects of screening in the photon propagator. In momentum space, the latter reads

$$D(\omega, \mathbf{k}) \approx D(0, \mathbf{k}) = \frac{i}{\epsilon_0 [k + \Pi(0, \mathbf{k})]}, \quad (16)$$

where ϵ_0 is the dielectric constant, associated with the substrate. When the value of ϵ_0 is large, the underlying dynamics becomes weakly coupled and the approximation for the gap equation (15) should become reliable. This is not always the case in graphene. However, we expect that this may be applicable in the case of the highest quality graphene devices, fabricated on a thin hexagonal boron nitride substrate²³.

A convenient explicit form of the polarization function in the presence of an external magnetic field was calculated in Refs.⁴⁹. In the approximation that neglects the wavefunction renormalization and the Dirac masses, it reads

$$\Pi(0, \mathbf{k}) = \frac{e^2 N_f}{16\pi l^2 T} \sum_{n=0}^{\infty} \sum_{\lambda=\pm} \frac{Q_{nn}^{\lambda\lambda}(y)}{\cosh^2(\frac{\mu - \lambda M_n}{2T})} - \frac{e^2 N_f}{4\pi l^2} \sum_{\substack{n,n'=0 \\ \lambda n \neq \lambda' n'}}^{\infty} \sum_{\lambda, \lambda'=\pm} Q_{nn'}^{\lambda\lambda'}(y) \frac{n_F(\lambda M_n) - n_F(\lambda' M_{n'})}{\lambda M_n - \lambda' M_{n'}} \quad (17)$$

where $M_n = \sqrt{2nv_F^2/l^2}$, T is the temperature, and the explicit form of function $Q_{n,n'}^{\lambda,\lambda'}(y)$ is given by⁴⁹

$$Q_{n,n'}^{\lambda,\lambda'}(y) = e^{-y} y^{|n-n'|} \left(\sqrt{\frac{(1 + \lambda\lambda'\delta_{0n>})n_{<}!}{n_{>}!}} L_{n_{<}}^{|n-n'|}(y) + \lambda\lambda'(1 - \delta_{0n<}) \sqrt{\frac{(n_{<} - 1)!}{(n_{>} - 1)!}} L_{n_{<-1}}^{|n-n'|}(y) \right)^2. \quad (18)$$

Here, by definition, $y = \mathbf{k}^2 l^2 / 2$, $n_> = \max(n, n')$ and $n_< = \min(n, n')$. We note that neglecting the wavefunction renormalization and masses in the calculation of the polarization function should provide a reasonable approximation to leading order in weak coupling. Moreover, this may work also at moderate coupling because the bulk of the polarization effects appear to be determined by the total number of filled Landau levels and not as much by the details of the quasiparticle dispersion relations.

For the derivation of the GLLR form of the gap equations, we refer the reader to Appendix B in Ref.⁴⁸. The final set of equations reads

$$\begin{aligned} \mu_{n,\sigma} - \mu_e - \sigma \tilde{\Delta}_{n,\sigma} = & \frac{\alpha \epsilon_l}{2} \sum_{n'=0}^{\infty} \kappa_{n',n}^{(0)} \left\{ n_F(E_{n',\sigma} - \mu_{n',\sigma}) - n_F(E_{n',\sigma} + \mu_{n',\sigma}) \right. \\ & \left. - \frac{\sigma \tilde{\Delta}_{n',\sigma}}{E_{n',\sigma}} [n_F(\mu_{n',\sigma} - E_{n',\sigma}) - n_F(E_{n',\sigma} + \mu_{n',\sigma})] \right\}, \end{aligned} \quad (19)$$

for $n \geq 0$, and

$$\begin{aligned} \mu_{n,\sigma} - \mu_e + \sigma \tilde{\Delta}_{n,\sigma} = & \frac{\alpha \epsilon_l}{2} \sum_{n'=1}^{\infty} \kappa_{n'-1,n-1}^{(0)} \left\{ n_F(E_{n',\sigma} - \mu_{n',\sigma}) - n_F(E_{n',\sigma} + \mu_{n',\sigma}) \right. \\ & \left. + \frac{\sigma \tilde{\Delta}_{n',\sigma}}{E_{n',\sigma}} [n_F(\mu_{n',\sigma} - E_{n',\sigma}) - n_F(E_{n',\sigma} + \mu_{n',\sigma})] \right\}, \end{aligned} \quad (20)$$

$$f_{n,\sigma} = 1 + \frac{\alpha \epsilon_l}{2} \sum_{n'=1}^{\infty} \frac{\kappa_{n'-1,n-1}^{(1)}}{n} \frac{f_{n',\sigma}}{E_{n',\sigma}} [n_F(\mu_{n',\sigma} - E_{n',\sigma}) - n_F(E_{n',\sigma} + \mu_{n',\sigma})], \quad (21)$$

$$g_{n,\sigma} = \frac{\alpha \epsilon_l}{2} \sum_{n'=1}^{\infty} \frac{\kappa_{n'-1,n-1}^{(1)}}{n} \frac{g_{n',\sigma}}{E_{n',\sigma}} [n_F(\mu_{n',\sigma} - E_{n',\sigma}) - n_F(E_{n',\sigma} + \mu_{n',\sigma})], \quad (22)$$

for $n \geq 1$. In these equations, we introduced a dimensionless coupling constant, $\alpha \equiv e^2 / \epsilon_0 v_F \approx 2.2$, which is an analog of the fine structure constant for suspended graphene.

The effect of screening in the above set of gap equations is implicit. It comes only through the modified values of the kernel coefficients⁴⁸,

$$\kappa_{m,n}^{(\rho)} = \int_0^\infty \frac{dk}{2\pi} \frac{kl \mathcal{L}_{m,n}^{(\rho)}(kl)}{k + \Pi(0, k)}, \quad \text{with } \rho = 0, 1. \quad (23)$$

It is straightforward to calculate numerically the static polarization function $\Pi(0, k)$ as a function of dimensionless variable kl . We checked that, for sufficiently small and sufficiently large values of kl , the numerical results approach the expected asymptotical behavior at $k \rightarrow 0$ and $k \rightarrow \infty$, respectively, derived in Eqs. (19) and (22) in Ref.⁴⁹. Then, by making use of the definition in Eq. (23), we obtain the numerical values of the kernel coefficients $\kappa_{m,n}^{(\rho)}$ (with $\rho = 0, 1$). The results for the first few Landau levels are presented in Tables I and II, respectively. By comparing these with the kernel coefficients in Ref.⁴⁸, we observe that the screening effects substantially (i.e., by about a factor of 2) decrease the values of $\kappa_{m,n}^{(\rho)}$. As we will see in the next section, this change strongly affects the magnitude of the order parameters (i.e., the symmetry breaking Dirac masses and chemical potentials) in the QH states with fractional filling of Landau levels.

III. NUMERICAL RESULTS

In this section, we present our numerical solutions to the GLLR gap equations (19) through (22) in the model with static screening effects. In the calculation, we use the Newtonian iteration algorithm and replace an original infinite set of gap equations with a truncated set of $n_{\max} = 50$ equations. In accordance with such a truncation, we also impose a sharp cutoff in the summation over the Landau level index at $n_{\max} = 50$. (The numerical tests reveal that the cutoff at $n_{\max} = 100$ does not affect any qualitative features of the solutions and only slightly changes the numerical results for the dynamical parameters in the first few Landau levels.)

Taking into account that each Landau level ($n \leq n_{\max}$) has 2 possible spin states and each of them is characterized by 8 different dynamical parameters, see Eq. (10), we have a total of $16n_{\max}$ independent parameters that should be determined by solving $16n_{\max}$ coupled algebraic equations, see Eq. (19) through (22). [Strictly speaking the number

TABLE I. The kernel coefficients $\kappa_{m,n}^{(0)}$ with the effects of static screening included.

$\kappa_{m,n}^{(0)}$	$m = 0$	$m = 1$	$m = 2$	$m = 3$	$m = 4$	$m = 5$	$m = 6$	$m = 7$	$m = 8$	$m = 9$	$m = 10$
0	0.0744	0.0235	0.0164	0.0136	0.0120	0.0109	0.0101	0.0094	0.0088	0.0083	0.0079
1	0.0235	0.0602	0.0222	0.0156	0.0129	0.0114	0.0104	0.0096	0.0090	0.0085	0.0081
2	0.0164	0.0222	0.0531	0.0211	0.0149	0.0124	0.0109	0.0100	0.0093	0.0087	0.0083
3	0.0136	0.0156	0.0211	0.0486	0.0202	0.0144	0.0120	0.0106	0.0097	0.0090	0.0085
4	0.0120	0.0129	0.0149	0.0202	0.0453	0.0195	0.0140	0.0116	0.0103	0.0094	0.0088
5	0.0109	0.0114	0.0124	0.0144	0.0195	0.0428	0.0189	0.0137	0.0113	0.0100	0.0092
6	0.0101	0.0104	0.0109	0.0120	0.0140	0.0189	0.0407	0.0184	0.0133	0.0111	0.0098
7	0.0094	0.0096	0.0100	0.0106	0.0116	0.0137	0.0184	0.0390	0.0180	0.0131	0.0109
8	0.0088	0.0090	0.0093	0.0097	0.0103	0.0113	0.0133	0.0180	0.0375	0.0176	0.0128
9	0.0083	0.0085	0.0087	0.0090	0.0094	0.0100	0.0111	0.0131	0.0176	0.0362	0.0172
10	0.0079	0.0081	0.0083	0.0085	0.0088	0.0092	0.0098	0.0109	0.0128	0.0172	0.0351

TABLE II. The kernel coefficients $\kappa_{m,n}^{(1)}$ with the effects of static screening included.

$\kappa_{m,n}^{(1)}$	$m = 0$	$m = 1$	$m = 2$	$m = 3$	$m = 4$	$m = 5$	$m = 6$	$m = 7$	$m = 8$	$m = 9$	$m = 10$
0	0.0509	0.0142	0.0084	0.0064	0.0055	0.0051	0.0048	0.0046	0.0043	0.0041	0.0039
1	0.0142	0.0901	0.0283	0.0172	0.0131	0.0111	0.0099	0.0093	0.0088	0.0084	0.0081
2	0.0084	0.0283	0.1244	0.0419	0.0260	0.0198	0.0167	0.0148	0.0137	0.0129	0.0123
3	0.0064	0.0172	0.0419	0.1553	0.0550	0.0346	0.0264	0.0222	0.0197	0.0181	0.0169
4	0.0055	0.0131	0.0260	0.0550	0.1839	0.0677	0.0431	0.0330	0.0276	0.0244	0.0224
5	0.0051	0.0111	0.0198	0.0346	0.0677	0.2107	0.0801	0.0515	0.0395	0.0331	0.0292
6	0.0048	0.0099	0.0167	0.0264	0.0431	0.0801	0.2361	0.0922	0.0597	0.0459	0.0385
7	0.0046	0.0093	0.0148	0.0222	0.0330	0.0515	0.0922	0.2602	0.1039	0.0678	0.0523
8	0.0043	0.0088	0.0137	0.0197	0.0276	0.0395	0.0597	0.1039	0.2834	0.1154	0.0758
9	0.0041	0.0084	0.0129	0.0181	0.0244	0.0331	0.0459	0.0678	0.1154	0.3056	0.1266
10	0.0039	0.0081	0.0123	0.0169	0.0224	0.0292	0.0385	0.0523	0.0758	0.1266	0.3271

of independent parameters is $16n_{\max} + 4$, where the additional 4 corresponds to the $n = 0$ Landau level, which is special.]

Before proceeding with the numerical analysis, it is useful to note that the coupled sets of gap equations for the two spin states, $s = \downarrow, \uparrow$, have exactly the same form. They differ only in the value of the chemical potential, i.e., $\mu_{\uparrow} = \mu_e - Z$ and $\mu_{\downarrow} = \mu_e + Z$, where $Z \equiv \mu_B B$ is the Zeeman energy. We also note that the gap equations are the same for $\sigma = \pm 1$ when the dynamical parameters $f_{n,\sigma}$, $g_{n,\sigma}$, $\mu_{n,\sigma}$ and $\sigma \hat{\Delta}_{n,\sigma}$ are treated as independent variables. These two observations allow us to greatly reduce the numerical cost of calculations. We first consider the generic set of equations in a finite range of chemical potentials and tabulate possible solutions for the above-mentioned four independent parameters. Usually, there exist multiple solutions that differ in their symmetry properties. The final solutions for the complete set of dynamical parameters with fixed values of $s = \downarrow, \uparrow$ and $\sigma = \pm 1$ are obtained by combining the distinct generic solutions obtained at properly shifted values of the chemical potential.

In the numerical analysis, it is convenient to express all physical quantities in units of the Landau energy scale,

$$\epsilon_l = \sqrt{\hbar v_F^2 |eB_{\perp}|/c} \approx 26\sqrt{B_{\perp} [\text{T}]} \text{ meV} \approx 300\sqrt{B_{\perp} [\text{T}]} \text{ K}, \quad (24)$$

where the value of the magnetic field is measured in Teslas. It may be appropriate to emphasize here that, while ϵ_l is determined by the component of the magnetic field orthogonal to the plane of graphene \mathbf{B}_{\perp} , the Zeeman energy $Z = \mu_B B \approx 5.8 \times 10^{-2} B [\text{T}] \text{ meV} \approx 0.67 B [\text{T}] \text{ K}$ is proportional to the absolute value of \mathbf{B} . Despite the fact that $B_{\perp} \leq B$, the Zeeman energy is generically much smaller than the Landau energy scale (24). This changes only in the case when the magnetic field becomes nearly parallel to the plane of graphene, i.e., when $B_{\perp} \ll B$. In the analysis below, we do not consider such a limiting case. In general, the dimensionless Zeeman energy is given by $z \equiv Z/\epsilon_l = 2.2 \times 10^{-3} \sqrt{B [\text{T}]} / \cos \theta_B$, where θ_B is the angle of the magnetic field tilt. In the numerical analysis

TABLE III. Values of the wavefunction renormalization f_n for several values of the chemical potentials with screening effects considered, compared with the solutions in⁴⁸ with screening effects neglected in the parentheses. (Note that the corresponding data in Ref.⁴⁸ had typos that were corrected here.)

	f_1	f_2	f_3	f_4	f_5	f_6
$ \mu_e < \sqrt{2}\epsilon_l$	1.084 (1.270)	1.072 (1.243)	1.065 (1.227)	1.060 (1.214)	1.057 (1.205)	1.054 (1.197)
$\sqrt{2}\epsilon_l < \mu_e < \sqrt{4}\epsilon_l$	1.045 (1.194)	1.066 (1.224)	1.063 (1.217)	1.059 (1.208)	1.056 (1.201)	1.054 (1.194)
$\sqrt{4}\epsilon_l < \mu_e < \sqrt{6}\epsilon_l$	1.037 (1.166)	1.042 (1.177)	1.058 (1.200)	1.057 (1.199)	1.055 (1.194)	1.052 (1.189)
$\sqrt{6}\epsilon_l < \mu_e < \sqrt{8}\epsilon_l$	1.033 (1.150)	1.035 (1.156)	1.039 (1.165)	1.052 (1.184)	1.052 (1.185)	1.051 (1.182)
$\sqrt{8}\epsilon_l < \mu_e < \sqrt{10}\epsilon_l$	1.031 (1.138)	1.032 (1.142)	1.034 (1.148)	1.037 (1.156)	1.048 (1.172)	1.049 (1.174)
$\sqrt{10}\epsilon_l < \mu_e < \sqrt{12}\epsilon_l$	1.029 (1.128)	1.030 (1.132)	1.031 (1.136)	1.032 (1.141)	1.035 (1.148)	1.045 (1.162)
$\sqrt{12}\epsilon_l < \mu_e < \sqrt{14}\epsilon_l$	1.027 (1.121)	1.028 (1.123)	1.028 (1.127)	1.029 (1.130)	1.031 (1.135)	1.034 (1.141)

below, we will fix the value of the dimensionless Zeeman energy to be $z = 0.015$. This formally corresponds to $B/\cos\theta_B \approx 46.5$ T.

A. Fermi velocity renormalization in weak magnetic field

In a weak magnetic field, the effect of symmetry breaking dynamical parameters is expected to be negligible. However, even in this regime it is interesting to explore the implications of the long-range Coulomb interaction on the quantum Hall effect in graphene. In particular, the interaction is expected to renormalize the Fermi velocity, which can be extracted from the dynamically modified expressions for the Landau level energies⁴⁸. In absence of QHF and MC order parameters, as we see from Eq. (14), the energies are given by $E_n = f_n v_F \sqrt{2n\epsilon_l}$, implying that the renormalized Fermi velocity is determined by the wavefunction renormalization parameters f_n , namely $v_{n,F}^{(\text{ren})} \equiv f_n v_F$. Without screening of the Coulomb interaction, the numerical values for the wavefunction renormalization parameters f_n were previously reported in Ref.⁴⁸. The corresponding results with the effects of screening were reported in Ref.³⁵ for the QH states with filling factors $\nu = \pm 4(k + 1/2)$. In the latter study, in fact, the dynamical parameters μ_n and Δ_n were also properly accounted for. By noting that the values of f_n depend not only on the chemical potential, but also on the Landau level index n , we conclude that the same is also true for the renormalized Fermi velocity. This is a very interesting theoretical prediction that could be easily tested in optical experiments, for example, via a systematic study of absorption/transmission lines for each of the QH states^{51–53}.

In the context of the optical transitions, the effect of interactions can be conveniently quantified by measuring the deviations of the measured energies of transitions from the free theory predictions⁵²,

$$\Delta E_{n,n'} = E_{n'} \pm E_n = (\sqrt{2n'} \pm \sqrt{2n})\epsilon_l + \alpha\epsilon_l C_{n,n'}, \quad (25)$$

where the minus sign corresponds to transitions between states with negative energies and states with positive energies. Strictly speaking, the above definition of $\Delta E_{n,n'}$ assumes transitions between states with the same spin. In the case of transitions between different spin states, an extra $\pm 2Z$ correction should be added on the right hand side. Here, the information about the wavefunction renormalization is captured by the following set of dimensionless parameters $C_{n,n'}$, i.e.,

$$C_{n,n'} = \frac{\sqrt{2n'}}{\alpha}(f_{n'} - 1) \pm \frac{\sqrt{2n}}{\alpha}(f_n - 1). \quad (26)$$

As we see, in absence of symmetry breaking, which is the case in weak magnetic fields, the values of parameters $C_{n,n'}$ are directly related to the quasiparticle velocity renormalizations. As we claim here, for each QH state, the corresponding renormalizations are functions of the Landau level index n . In experiment, the complete set of parameters f_n with $n \geq 1$ could be extracted by measuring the transition energies between the lowest Landau level (which is free from the corresponding renormalization effect) and higher Landau levels. The values of f_n , extracted in this way, would be sufficient to calculate the values of $C_{n,n'}$ for transitions between various higher Landau levels. The latter could be also compared to the actual measurements and, in the case of agreement, one would have a nontrivial test of the self-consistency of the GLLR ansatz used here. From a theoretical point of view, it will be perhaps even more interesting if deviations from the relations in Eq. (26) are observed.

In a general case with nonvanishing QHF and MC order parameters, the expressions for $C_{n,n'}$ parameters should be corrected because the Landau level energies are modified, see Eqs. (13) and (14). The magnitude of the corresponding

TABLE IV. Parameters $C_{n,n'}$ in the QH state with the filling factor $\nu = 2$ in the model with static screening. The values in parentheses are obtained in an approximation with the wavefunction renormalization effects included, but all QHF and MC order parameters neglected.

$C_{n,n'}$	$n' = 1$	$n' = 2$	$n' = 3$	$n' = 4$
$n = 0$	0.082 (0.054)	0.093 (0.065)	0.099 (0.072)	0.103 (0.077)
$n = -1$	0.100 (0.108)	0.111 (0.119)	0.117 (0.126)	0.122 (0.131)
$n = -2$	0.108 (0.119)	0.119 (0.130)	0.125 (0.138)	0.129 (0.143)
$n = -3$	0.113 (0.126)	0.124 (0.138)	0.130 (0.144)	0.134 (0.150)
$n = -4$	0.116 (0.131)	0.127 (0.143)	0.133 (0.150)	0.138 (0.220)

TABLE V. Parameters $C_{n,n'}$ in the QH state with the filling factor $\nu = 6$ in the model with static screening. The values in parentheses are obtained in an approximation with the wavefunction renormalization effects included, but all QHF and MC order parameters neglected.

$C_{n,n'}$	$n' = 2$	$n' = 3$	$n' = 4$
$n = 1$	0.054 (0.031)	0.066 (0.041)	0.073 (0.047)
$n = 0$	0.088 (0.060)	0.100 (0.070)	0.107 (0.076)
$n = -1$	0.103 (0.089)	0.115 (0.100)	0.122 (0.105)
$n = -2$	0.109 (0.121)	0.121 (0.131)	0.128 (0.136)
$n = -3$	0.113 (0.131)	0.125 (0.141)	0.132 (0.147)
$n = -4$	0.116 (0.136)	0.128 (0.147)	0.135 (0.152)

corrections is of the order of $|\mu_{n,\sigma} - \mu_e|$ and $\tilde{\Delta}_{n,\sigma}^2/(\sqrt{n}\epsilon_l)$ for Landau levels $n \geq 1$. (Note that the correction due to the QHF order parameter should be interpreted as part of the energy measured with respect to the thermodynamical potential μ_e .) In the case of transitions to/from the lowest Landau level ($n = 0$), the corrections are $\pm\sigma\Delta_{0,\sigma}$, see Eq. (13). Below, we present our numerical results for the parameters $C_{n,n'}$ in several QH states in both approximations, i.e., with and without inclusion of the QHF and MC order parameters.

By utilizing the same value of the cutoff, $n_{\max} = 100$, in the numerical calculation as in⁴⁸, but also including the effects of screening, we straightforwardly obtain the wavefunction renormalization parameters f_n . The corresponding zero temperature results for the first few Landau levels are presented in Table III. We note that they differ slightly from those in Ref.³⁵ because here all dynamical parameters such as μ_n and Δ_n were neglected. For comparison, in Table III we also list in the parentheses the numerical results from Ref.⁴⁸, obtained without the screening effects. Different rows in Table III correspond to different choices of the chemical potential in the gaps between a completely filled n th Landau level and a completely empty $(n+1)$ th Landau level.

By comparing the results with and without screening in Table III, we find that the effect of wave function renormalization goes from about 14% to 27% down to about 3% to 8%, which appears to be even smaller than the prediction in Ref.⁵⁴. It is curious to explore in detail if the logarithmic running of the coupling constant could explain such a difference. By making use of the definition in Eq. (26) and our numerical results for various QH states, we readily calculate $C_{n,n'}$ parameters.

The representative results for $C_{n,n'}$ parameters are presented in Tables IV and V for the QH states with the filling factors $\nu = 2$ and $\nu = 6$. Because of the particle-hole symmetry, the results for the corresponding negative filling factors can be obtained as follows: $C_{n,n'}(-\nu) = C_{-n',-n}(\nu)$. These results appear to be about 2 to 4 times smaller than the results in the absence of screening⁴⁸. In calculation, we took into account the effect of nonvanishing QHF and MC order parameters. For comparison, in parenthesis we also show the results for the same parameters in the approximation with the QHF and MC order parameters neglected. It appears that the role of such parameters is not negligible.

B. Quantum Hall states in strong magnetic field

In this subsection, we study QH states with different integer filling factors at zero temperature. We will start by first considering the states associated with the $n = 0$ and $n = 1$ Landau levels. We will show, in particular, that the qualitative features of the phase diagram obtained in Ref.⁴⁸ remain qualitatively the same after the inclusion of the static screening. At the same time, the quantitative changes will be substantial.

TABLE VI. Gap parameters for the solutions when the Fermi energy close to the lowest Landau level. The solutions for $n_{\max} = 50$ with screening effects considered are compared with the solutions in⁴⁸ for $n_{\max} = 5$ neglecting screening effects in the parentheses.

ν	$\tilde{\Delta}_{0,\uparrow}^{\text{eff}}$	$\tilde{\Delta}_{0,\downarrow}^{\text{eff}}$	$\Delta_{0,\uparrow}$	$\Delta_{0,\downarrow}$
-2	0.000 (0.000)	0.000 (0.000)	0.082 (0.227)	0.082 (0.227)
-1	0.000 (0.000)	0.082 (0.227)	0.082 (0.227)	0.000 (0.000)
0	0.000 (0.000)	0.000 (0.000)	0.082 (0.227)	-0.082 (-0.227)
1	0.082 (0.227)	0.000 (0.000)	0.000 (0.000)	-0.082 (-0.227)
2	0.000 (0.000)	0.000 (0.000)	-0.082 (-0.227)	-0.082 (-0.227)

As stated earlier, the gap equations (19) through (22) allow a large number of solutions with different types of Haldane/Dirac masses ($\Delta_n, \tilde{\Delta}_n$) and chemical potentials ($\mu_n, \tilde{\mu}_n$). In order to identify the true ground state among them, we compare their free energies. [For the explicit expression of the free energy, see Appendix C in Ref.⁴⁸.] In the model at hand, the choice of the corresponding states is strongly affected by the Zeeman interaction energy, which is one of the main factors in driving the vacuum alignment. Taking into account that there may exist a large number of other symmetry breaking effects, e.g., various on-site repulsion interaction terms¹², the actual nature of the ground states should be accepted with caution. Nevertheless, the study below is quite informative: it reveals the quantitative effects of the static screening and role of the running of the dynamical parameters in the QH regime of graphene.

From the symmetry viewpoint, there are two types of Dirac masses and chemical potentials for quasiparticles of each spin orientation, $s = \downarrow, \uparrow$. The parameters of the first type (i.e., Δ_n and μ_n) are singlets, while the parameters of the second type (i.e., $\tilde{\Delta}_n$ and $\tilde{\mu}_n$) are triplets with respect to the flavor $U_s(2)$ subgroups. It is natural to expect that the states with different symmetry properties compete. However, it should be emphasized that the corresponding competition is not necessarily between the MC and QHF scenarios because both types of order parameters may belong to the same representations of the flavor symmetry. In fact, as our results show, the two types of order parameters generically coexist in all QH states. (This was also emphasized in Ref.⁴⁸.)

From general considerations based on the structure of the Landau levels, it is expected that there exist at least four different classes of QH states with the following series of filling factors: (i) $\nu = 4n + 2$, (ii) $\nu = 4n$ (with a possible exclusion of the rather unique $\nu = 0$ state in a class of its own), (iii) $\nu = 4n - 1$, and (iv) $\nu = 4n + 1$.

The first series of states with the filling factors $\nu = 4n + 2$ describes the “normal” QH states with the complete filling of the (nearly) degenerate Landau levels. They do not have or require symmetry breaking and are resolved even at relatively weak magnetic fields. The simplest realization of the $\nu = 4n$ states could be provided by a dynamically enhanced Zeeman splitting of Landau levels. In this case, the ground states have $U_\downarrow(2) \times U_\uparrow(2)$ symmetry. While this also the prediction of the model at hand, we should emphasize that other realizations of the $\nu = 4n$ QH states are possible. In fact, the $\nu = 0$ state, which formally belongs to this series, is likely to have a different origin⁴⁴. The remaining two series of states with the filling factors $\nu = 4n \pm 1$ are less controversial. They require spontaneous symmetry breaking at least down to $U_\downarrow(1) \times U_\uparrow(2)$ or $U_\downarrow(2) \times U_\uparrow(1)$.

In our analysis at sufficiently small values of the chemical potential, we find a number of different solutions, associated with the lowest Landau level ($n = 0$) and integer filling factors $\nu = 0, \pm 1, \pm 2$. The order of appearance and the competition of different types of solutions appear to be the same as in Ref.⁴⁸, see Figure 3 there. By taking into account the screening of the Coulomb interaction, however, we find that the actual values of dynamical parameters change substantially. The corresponding results are listed in Table VI. For comparison, in parenthesis we also list the previous results in the model without screening⁴⁸. As we see, the effect of screening is to suppress the relevant dynamical parameters by about a factor of 3. The same is true for the magnitude of the energy gaps in the states with the filling factors $\nu = 0, \pm 1$.

The analysis of the QH states, associated with the $n = 1$ Landau level, is done in the same way. Here again, the order of appearance and the competition of different types of solutions appear to be exactly the same as in Ref.⁴⁸, see Figure 4 there. The actual values of the dynamical parameters in the model with screening are listed in Table VII. The corresponding results in the model without screening are given in parenthesis. By comparing the two sets of data, we find that screening leads to a suppression of the relevant dynamical parameters by a factor of 3 to 5.

Because of the long-range nature of the Coulomb interaction, the dynamical QHF ($\mu_n, \tilde{\mu}_n$) and MC ($\Delta_n, \tilde{\Delta}_n$) order parameters are nontrivial functions of the Landau level index n . The corresponding “running” of the dynamical parameters is an important feature of the model at hand. From theoretical viewpoint, it is essential to provide a realistic description of the low-energy dynamics in graphene, where the role of order parameters diminishes with increasing the quasiparticle energy. This is in contrast to a common mean-field analysis of models with point-like interactions, where the order parameters affect either (i) only the nearest filled Landau level or (ii) all levels in the

TABLE VII. Gap parameters for the solutions when the Fermi energy close to the Landau level at $n = 1$. The solutions for $n_{\max} = 50$ with screening effects considered are compared with the solutions in⁴⁸ for $n_{\max} = 5$ neglecting screening effects in the parentheses.

	spin	$\tilde{\Delta}_0^{\text{eff}}$	Δ_0	f_1	$\mu_1 - \mu_s$	Δ_1	$\tilde{\Delta}_1$	f_2	$\mu_2 - \mu_s$	Δ_2	$\tilde{\Delta}_2$
$\nu = 3$	\uparrow	0.000 (0.000)	-0.082 (-0.227)	1.078 (1.143)	0.013 (0.053)	-0.014 (-0.068)	0.000 (0.000)	1.065 (1.112)	0.009 (0.040)	-0.010 (-0.052)	0.000 (0.000)
	\downarrow	-0.013 (-0.051)	-0.095 (-0.278)	1.058 (1.105)	0.050 (0.148)	-0.010 (-0.049)	0.004 (0.018)	1.062 (1.102)	0.022 (0.091)	-0.009 (-0.046)	0.000 (0.006)
$\nu = 4$	\uparrow	0.000 (0.000)	-0.082 (-0.227)	1.078 (1.143)	0.013 (0.053)	-0.014 (-0.068)	0.000 (0.000)	1.065 (1.112)	0.009 (0.040)	-0.010 (-0.052)	0.000 (0.000)
	\downarrow	0.000 (0.000)	-0.108 (-0.330)	1.038 (1.066)	0.087 (0.243)	-0.006 (-0.031)	0.000 (0.000)	1.059 (1.093)	0.034 (0.143)	-0.009 (-0.039)	0.000 (0.000)
$\nu = 5$	\uparrow	-0.013 (-0.051)	-0.095 (-0.278)	1.058 (1.105)	0.049 (0.148)	-0.010 (-0.049)	0.004 (0.018)	1.062 (1.102)	0.021 (0.091)	-0.009 (-0.046)	0.000 (0.006)
	\downarrow	0.000 (0.000)	-0.108 (-0.278)	1.038 (1.066)	0.087 (0.245)	-0.006 (-0.031)	0.000 (0.000)	1.059 (1.093)	0.034 (0.143)	-0.009 (-0.039)	0.000 (0.000)
$\nu = 6$	\uparrow	0.000 (0.000)	-0.108 (-0.330)	1.038 (1.066)	0.087 (0.243)	-0.006 (-0.031)	0.000 (0.000)	1.059 (1.093)	0.034 (0.142)	-0.009 (-0.039)	0.000 (0.000)
	\downarrow	0.000 (0.000)	-0.108 (-0.331)	1.038 (1.066)	0.087 (0.245)	-0.006 (-0.031)	0.000 (0.000)	1.059 (1.093)	0.034 (0.143)	-0.009 (-0.039)	0.000 (0.000)

same way.

Our numerical results for the running dynamical parameters $f_{n,s}$, $\mu_{n,s}$, $\Delta_{n,s}$, $\tilde{\mu}_{n,s}$, and $\tilde{\Delta}_{n,s}$ are shown in Fig. 1 through Fig. 4. In line with our discussion of the four different classes of QH states with different filling factors, we show the results for $\nu = 4n + 2$, $\nu = 4n$, $\nu = 4n - 1$, and $\nu = 4n + 1$ states in separate panels. They are characterized by different ground state symmetries. In order to avoid overcrowding the figures, we showed the results only for a few states in the series, that correspond to partially or fully filled $n = 0$, $n = 1$, and $n = 2$ Landau levels. It is natural to expect that the other states in the same series, associated with filling of higher Landau levels, share essentially the same qualitative features.

In Figs. 1 – 4, the results for the spin-up and spin-down quasiparticle states are represented by the same types of filled and unfilled symbols, respectively. The universal property of all dynamical parameters is that their values approach the free model limit at large n . Additionally, we see that often the running parameters acquire their largest absolute values in the Landau levels near the Fermi energy. These features were expected, of course.

The results for the wavefunction renormalization parameters $f_{n,s}$ as functions of n are shown in Fig. 1. As we see, the results are qualitatively the same for all four different classes of QH states. This suggests that the wavefunction renormalization parameters and, thus, the renormalized Fermi velocities are largely determined by the long-range (screened) Coulomb interaction and not very sensitive to the effects of the dynamically generated symmetry breaking terms.

In the states with the even filling factors $\nu = 4n$ and $\nu = 4n + 2$, only the singlet order parameters $\mu_{n,\downarrow} - \mu_{n,\uparrow}$ and $\Delta_{n,s}$ are generated. In both cases, the dynamical parameters have comparable magnitudes and the ground state symmetry is $U_{\uparrow}(2) \times U_{\downarrow}(2)$. While the role of nontrivial $\mu_{n,\downarrow} - \mu_{n,\uparrow}$ and $\Delta_{n,s}$ is critical in the series of states with the filling factors $\nu = 4n$, it is not the case for the states with $\nu = 4n + 2$. Indeed, in the $\nu = 4n$ states, it is the singlet order parameters that determine the energy gaps of the QH states. They are critical because the corresponding dynamical energy gaps are generated to be much larger than the bare Zeeman splitting. This is in contrast to the $\nu = 4n + 2$ states, which are characterized by rather large gaps (of order ϵ_l) between Landau levels, which cannot be affected substantially by relatively small corrections due to $\mu_{n,\downarrow} - \mu_{n,\uparrow}$ and $\Delta_{n,s}$.

Our results for the $\nu = 4n$, associated with higher Landau levels, appear to be in qualitative agreement with the experimental results reported in Refs.^{23,25}. A spin polarized nature of the corresponding states is supported by the observed increase of the activation gaps as functions of the in-plane component of the magnetic field.

In agreement with our general symmetry arguments, the triplet order parameters $\tilde{\mu}_{n,s}$ and $\tilde{\Delta}_{n,s}$ are generated only in the states with the odd filling factors $\nu = 4n \pm 1$, see Fig. 4. We should note, however, that in both types of states

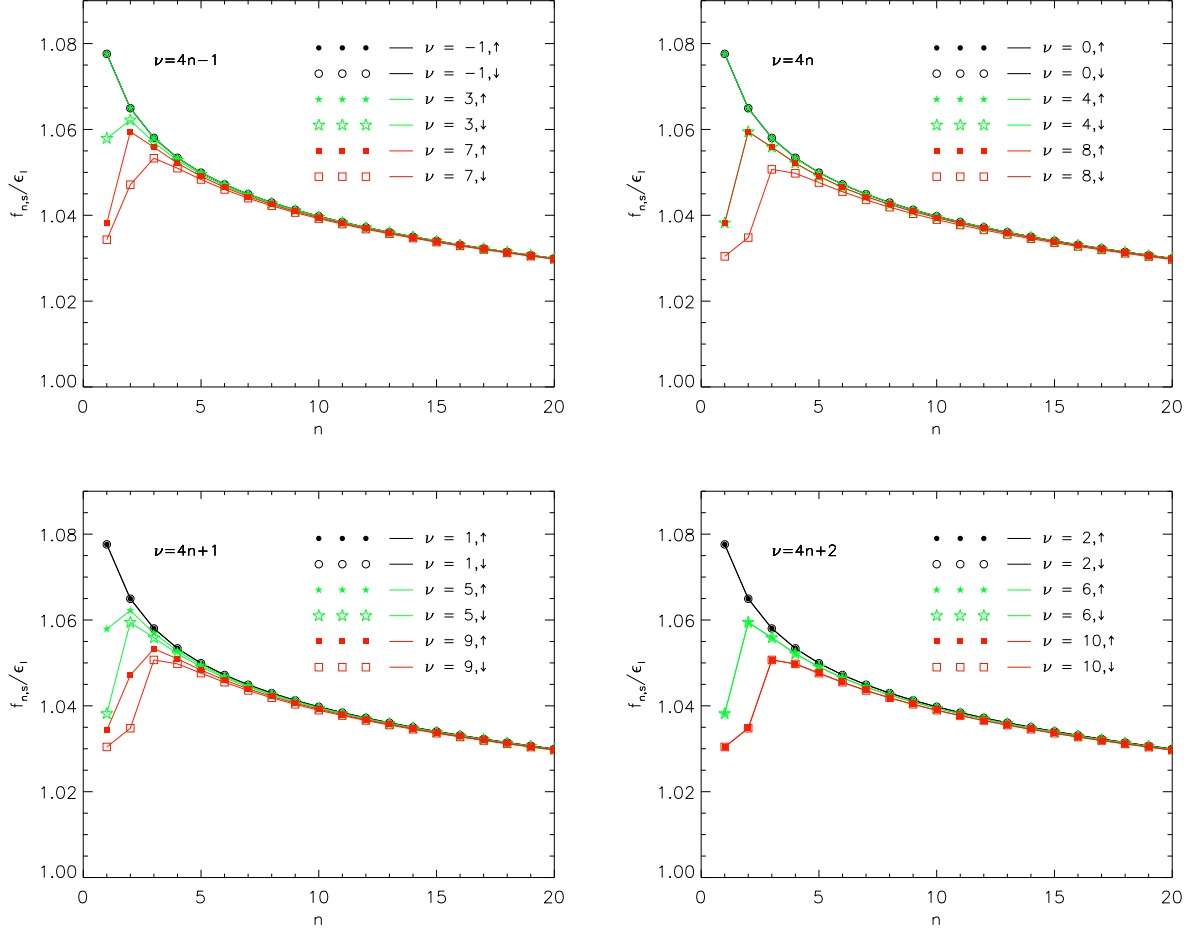


FIG. 1. (Color online) The wavefunction renormalization parameters $f_{n,s}$ as functions of the Landau level index n for four different types of QH states with filling factors $\nu = 4n - 1$, $\nu = 4n$, $\nu = 4n + 1$, and $\nu = 4n + 2$.

the singlet order parameters $\mu_{n,\downarrow} - \mu_{n,\uparrow}$ and $\Delta_{n,s}$ are generated as well, see Figs. 2 and 3. This is not surprising since they do not break any additional symmetries. The qualitative difference between the states with $\nu = 4n - 1$ and $\nu = 4n + 1$ is that the triplet order parameters are generated either exclusively for the spin-down quasiparticles ($\nu = 4n - 1$) or exclusively for the spin-up quasiparticles ($\nu = 4n + 1$). It is not immediately clear whether these results are in perfect agreement with the experimental data in Ref.²³. Our theoretical model appears to capture some of the key qualitative features of the experimental data. For example, the corresponding states are characterized by a spontaneous breakdown of the flavor symmetry and the gaps are not particularly sensitive to the Zeeman energy. On the other hand, the exact symmetry breaking pattern in the observed states with filling factors $\nu = 4n \pm 1$ is not clear. In theory, the ground state symmetry is either $U_{\downarrow}(1) \times U_{\uparrow}(2)$ or $U_{\downarrow}(2) \times U_{\uparrow}(1)$. While this does not contradict the measurements, the actual symmetry could in principle be lower, i.e., $U_{\downarrow}(1) \times U_{\uparrow}(1)$. One way to resolve the issue unambiguously is to investigate the spectrum of quasiparticles in detail, e.g., by studying systematically all allowed optical transitions. We hope that this will be done in future investigations.

C. Temperature dependence of the energy gaps

As is clear from our discussion in the previous subsection, the QH states with the filling factors $\nu = 4n$ and $\nu = 4n \pm 1$ are characterized by the energy gaps that are largely determined by the dynamically generated QHF and MC order parameters. (Recall that the energy gaps in the $\nu = 4n + 2$ states are of the order of the Landau energy scale ϵ_l and, thus, are not affected much by the dynamical order parameters.) The corresponding parameters and, therefore, the energy gaps are expected to have a strong temperature dependence. In this subsection, we study such

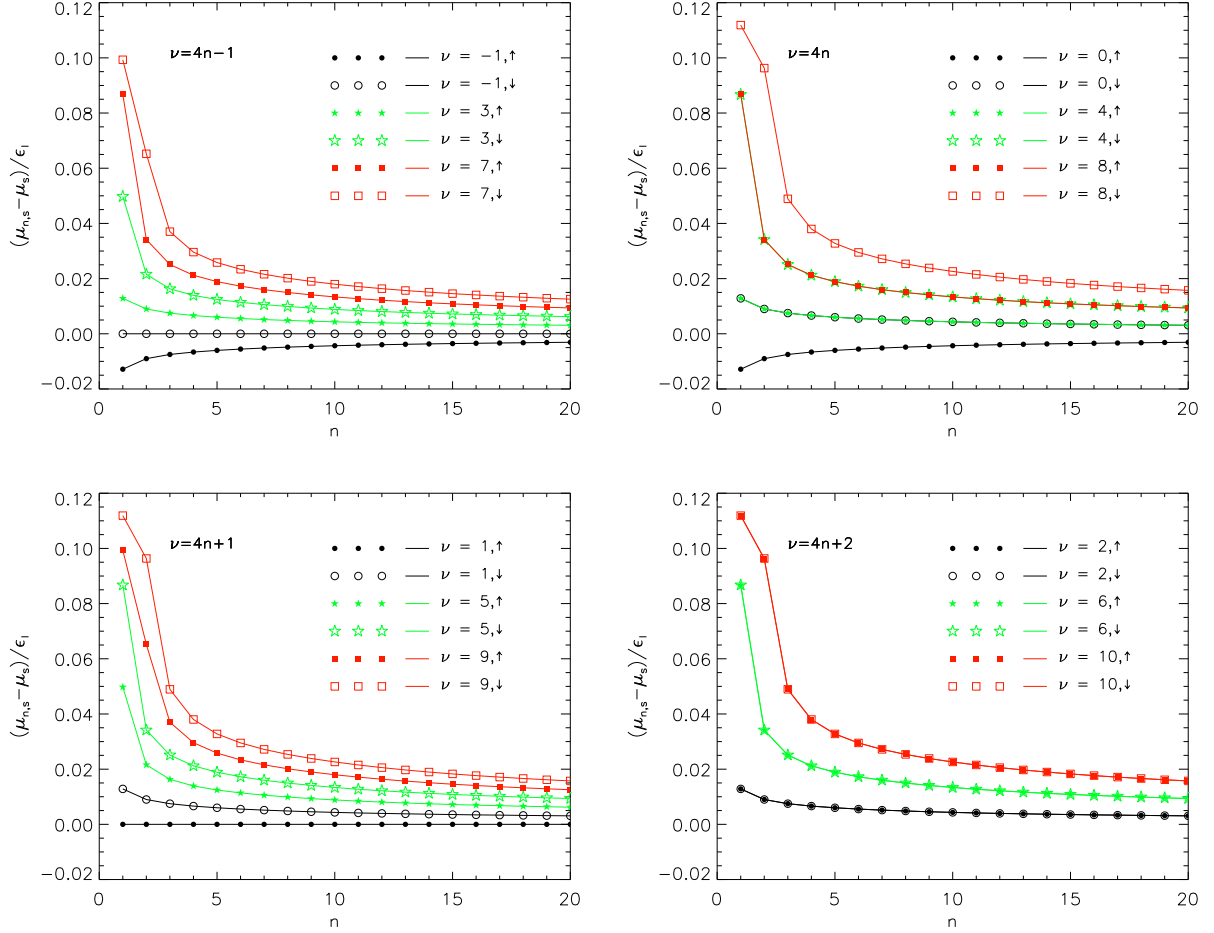


FIG. 2. (Color online) The chemical potential differences $\mu_{n,s} - \mu_s$ as functions of the Landau level index n for four different types of QH states with filling factors $\nu = 4n - 1$, $\nu = 4n$, $\nu = 4n + 1$, and $\nu = 4n + 2$.

a dependence in detail.

The numerical analysis of the GLLR gap equations (19) through (22) at nonzero temperature is qualitatively the same as at $T = 0$. After determining the ground states at various filling factors as a function of temperature, we can straightforwardly extract the temperature dependence of the energy gaps. For different types of the QH states, associated with various fillings of the lowest three Landau levels ($n = 0, 1, 2$), our numerical results are shown in Figs. 5 and 6. There are several universal features of these results: (i) the gaps decrease monotonically with temperature, (ii) the overall size of the gaps decreases with increasing n . We also find that, for a fixed n , the gap functions in the states with $\nu = 4n - 1$ and $\nu = 4n + 1$ are almost exactly the same, see Fig. 5.

By comparing the results in Fig. 6 with those in Fig. 5, we see that the temperature dependence of the energy gaps in the QH states with filling factors $\nu = 4n \pm 1$ is qualitatively different from that in the $\nu = 4n$ states. By taking into account the very different symmetry properties of the corresponding ground states, this is not surprising at all. The $\nu = 4n \pm 1$ states are characterized by the triplet order parameters $\tilde{\mu}_{n,s}$ and $\tilde{\Delta}_{n,s}$, which vanish in a symmetry restoring phase transition at the critical temperature T_c , see Fig. 5. The transition appears to be either a second-order, or a weakly first-order transition. The temperature dependence of the energy gaps in the $\nu = 4n \pm 1$ states is fitted quite well by the following function:

$$\Delta E = \Delta E^{(0)} \left[1 - \left(\frac{T}{T_c} \right)^4 \right]^{0.8}, \quad (27)$$

where $\Delta E^{(0)}$ is the energy gap at zero temperature and T_c is the critical temperature. Note that the approximate numerical values of the zero temperature gaps are $0.165\epsilon_l$, $0.130\epsilon_l$ and $0.112\epsilon_l$ for the $\nu = 4n \pm 1$ states, associated

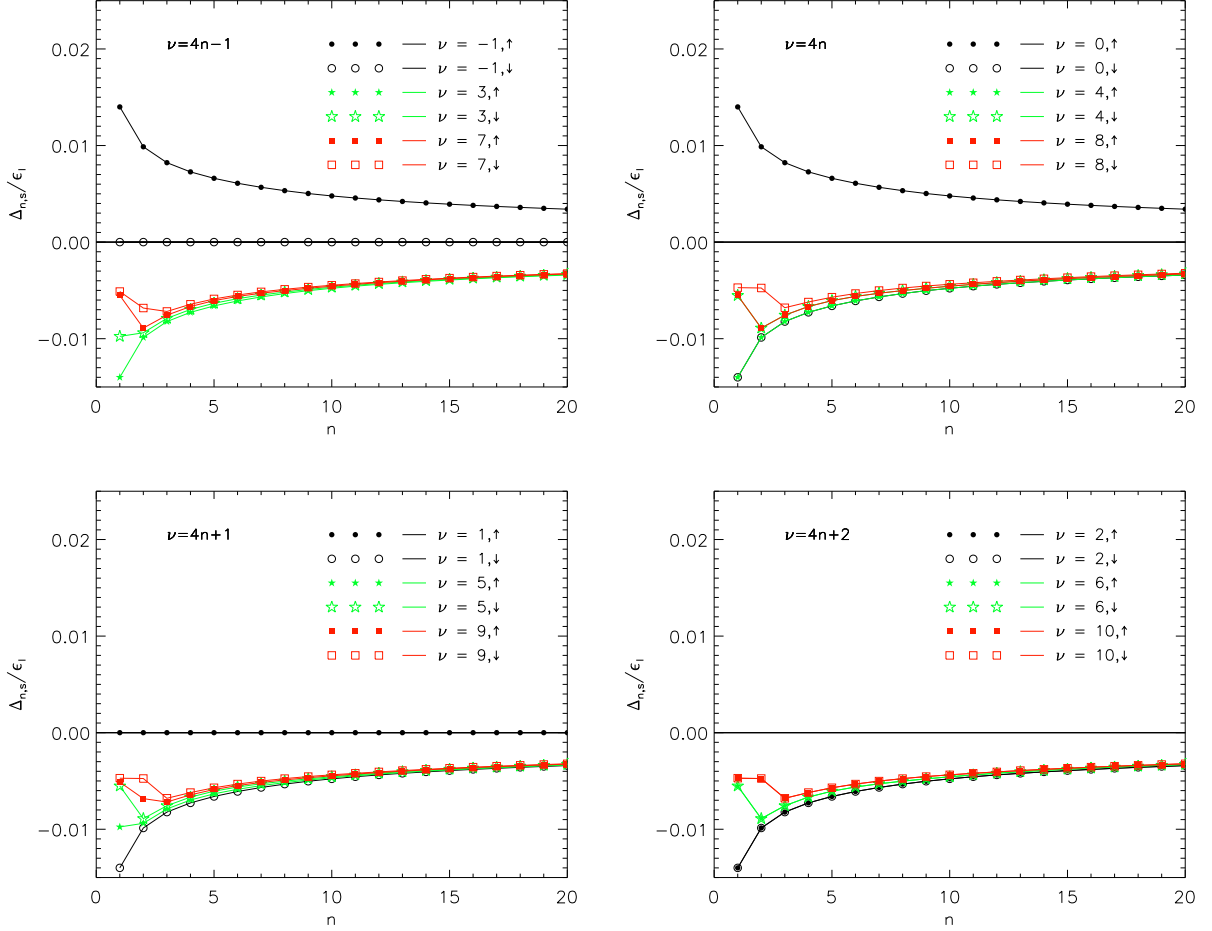


FIG. 3. (Color online) The singlet Haldane masses $\Delta_{n,s}$ as functions of the Landau level index n for four different types of QH states with filling factors $\nu = 4n - 1$, $\nu = 4n$, $\nu = 4n + 1$, and $\nu = 4n + 2$.

with the Landau levels $n = 0, 1, 2$, respectively. The corresponding approximate values of the critical temperatures are $0.043\epsilon_l$, $0.033\epsilon_l$ and $0.029\epsilon_l$, respectively.

In contrast, the $\nu = 4n$ states are characterized by the singlet order parameters $\mu_{n,\downarrow} - \mu_{n,\uparrow}$ and $\Delta_{n,s}$, which have the same symmetry as the Zeeman term and, thus, remain nonzero even at large temperatures, see Fig. 6. As a result, the corresponding transitions from the low-temperature $\nu = 4n$ states with a dynamically enhanced Zeeman splitting to the high-temperature states without such an enhancement are generically smooth crossovers. In the case of the $\nu = 0$ state, however, we find a sign of a small discontinuity in the temperature dependence of the energy gap around $T \simeq 0.04\epsilon_l$, suggesting a weak first-order transition. Of course, such a transition is not related to a restoration of any exact symmetry and, thus, can be viewed as accidental.

IV. DISCUSSION

In this paper, we utilized a highly flexible GLLR representation for the fermion propagator to describe the QH states with integer filling factors in the low-energy model of graphene with long-range Coulomb interaction. By including the static screening effects in an external magnetic field, we amended the earlier study of Ref.⁴⁸. While using a similar mean-field approximation, we found that the static screening has a substantial suppression effect on the dynamical order parameters in all QH states with spontaneously broken symmetry. Also, the deviations of the wavefunction renormalization from 1 and the dynamical corrections to the Fermi velocity became noticeably suppressed.

By making use of the framework that naturally incorporates the running of the dynamical parameters with the Landau level index n , we observed that the largest absolute values of such parameters are typically obtained for the

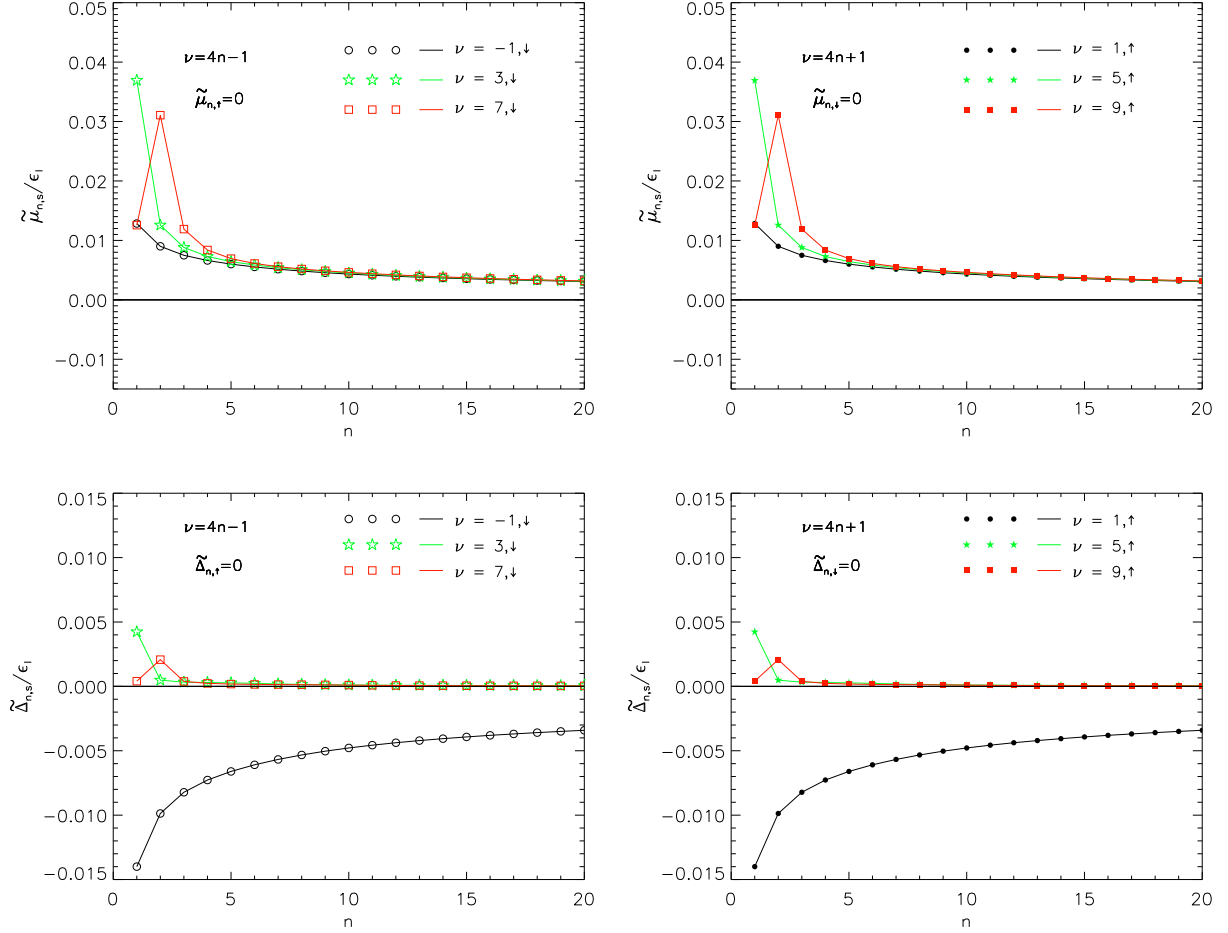


FIG. 4. (Color online) The triplet chemical potentials $\tilde{\mu}_{n,s}$ and the Dirac masses $\tilde{\Delta}_{n,s}$ as functions of the Landau level index n for the QH states with the filling factors $\nu = 4n \pm 1$.

Landau level near the Fermi energy. In the limit of large n , all dynamical parameters approach the corresponding bare values. By making use of numerical methods, we studied in detail the behavior of the dynamical parameters in all four different types of the QH states with the filling factors $\nu = 4n + 2$, $\nu = 4n$, and $\nu = 4n \pm 1$ that have different symmetry properties. At weak fields, we also analyze the running of the renormalized Fermi velocity with the Landau level index n .

In the low-energy model used, the states with the filling factors $\nu = 4n + 2$ and $\nu = 4n$ have the $U_{\uparrow}(2) \times U_{\downarrow}(2)$ symmetry. They are characterized by the singlet type of the QHF and MC order parameters with respect to $U_s(2)$ for both $s = \downarrow$ and $s = \uparrow$. While the role of the corresponding singlet parameters in the $\nu = 4n + 2$ states is negligible, it is profound in the $\nu = 4n$ states, where they determine the magnitude of the dynamically enhanced Zeeman splitting. This finding qualitatively agrees with the data reported in Refs.^{23,25}, which supports spontaneous symmetry breaking and spin polarization in $\nu = 4n$ states. The states with the odd filling factors $\nu = 4n \pm 1$ have rather different properties and are characterized by a lower ground state symmetry, i.e., either $U_{\uparrow}(1) \times U_{\downarrow}(2)$ or $U_{\uparrow}(2) \times U_{\downarrow}(1)$. In such states, in addition to the singlet order parameters, there are two types of spontaneously generated triplet parameters. The latter play a critical role in the realization of the $\nu = 4n \pm 1$ states by reducing the symmetry so as to allow the appropriate lifting of the fourfold degeneracy, as well as needed partial filling of Landau levels. These properties appear to be in agreement with the experimental data in Ref.²³, even though the data was not sufficient to establish unambiguously the underlying symmetry breaking pattern.

By extending the analysis to the case of nonzero temperature, we studied the energy gaps in the QH states with the filling factors $\nu = 4n$ and $\nu = 4n \pm 1$. We found that the symmetry breaking (triplet) order parameters, describing the $\nu = 4n \pm 1$ states, vanish at a certain critical value of temperature T_c , where a second-order or weakly first-order transition occurs. In terms of the zero temperature gap $\Delta E^{(0)}$, the results for the critical temperature are

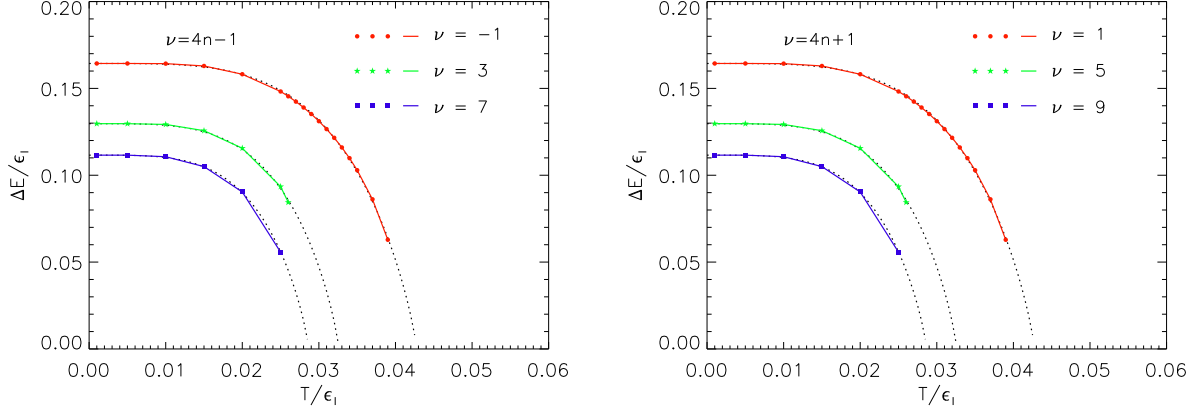


FIG. 5. (Color online) The energy gaps as functions of temperature for the QH states with the filling factors $\nu = 4n \pm 1$.

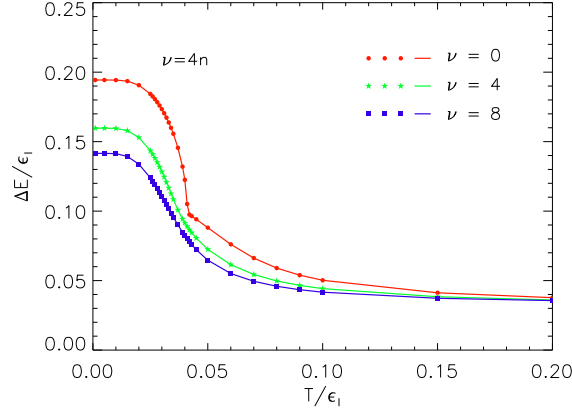


FIG. 6. (Color online) The energy gaps as functions of temperature for the QH states with the filling factors $\nu = 4n$.

approximately given by $T_c \approx 0.26\Delta E^{(0)}$ for all $\nu = 4n \pm 1$ states associated with filling of the first few Landau levels. On the other hand, we do not detect a well-defined symmetry-restoring phase transition in the temperature dependence of the energy gaps in the $\nu = 4n$ states. Instead, we find a smooth crossover, which is consistent with the fact that the corresponding states have no real symmetry-breaking order parameters.

The results of this study unambiguously suggest that the QH states of graphene with various integer filling factors are generically characterized by a rather large number of dynamical parameters that have a nontrivial running with the Landau level index n . The corresponding rich structure of Landau levels in the QH regime could be probed in detail via a systematic study of transition lines in optical experiments such as those reported in Refs.^{51–53}. The temperature dependence of the energy gaps obtained in this study appears to be in a qualitative agreement with the measurements of the activation energies in Ref.^{13,15,16,19,20,23,24}. While such an agreement is encouraging, it remains to be seen whether the theoretical predictions of the GLLR formalism could be matched quantitatively to the experimental data. Before such a comparison is attempted, however, one may need to reevaluate the model approximations used in the present study. In particular, one should address the precise quantitative role of (i) dynamical screening, (ii) fluctuations of the order parameter fluctuations, and (iii) nonzero quasiparticles widths. Hopefully, all such effects in GLLR formalism will be addressed in the future studies.

ACKNOWLEDGMENTS

The authors acknowledge participation of Yingchao Lu during the early stages of this project. The authors thank E. V. Gorbar for numerous discussions and useful comments on the text of the paper. This work was supported by

the U.S. National Science Foundation under Grant No. PHY-1404232.

-
- * igor.shovkovy@asu.edu
† lifang.xia@asu.edu
- ¹ G. W. Semenoff, Phys. Rev. Lett. **53**, 2449 (1984).
 - ² D. P. DiVincenzo and E. J. Mele, Phys. Rev. B **29**, 1685 (1984).
 - ³ K. S. Novoselov, A. K. Geim, S. V. Morozov, D. Jiang, M. I. Katsnelson, I. V. Grigorieva, S. V. Dubonos, and A. A. Firsov, Nature **438**, 197 (2005).
 - ⁴ Y. Zhang, Y.-W. Tan, H. L. Stormer, and P. Kim, Nature **438**, 201 (2005).
 - ⁵ Y. Zheng and T. Ando, Phys. Rev. B **65**, 245420 (2002) 245420.
 - ⁶ E. V. Gorbar, V. P. Gusynin, V. A. Miransky and I. A. Shovkovy, Phys. Rev. B **66**, 045108 (2002).
 - ⁷ V. P. Gusynin and S. G. Sharapov, Phys. Rev. Lett. **95**, 146801 (2005); Phys. Rev. B **73**, 245411 (2006).
 - ⁸ N. M. R. Peres, F. Guinea, and A. H. Castro Neto, Phys. Rev. B **73**, 125411 (2006).
 - ⁹ A. H. Castro Neto, F. Guinea, N. M. R. Peres, K. S. Novoselov, and A. K. Geim, Rev. Mod. Phys. **81**, 109 (2009).
 - ¹⁰ D. S. L. Abergel, V. Apalkov, J. Berashevich, K. Ziegler, and T. Chakraborty, Adv. Phys. **59**, 261 (2010).
 - ¹¹ Y. Barlas, K. Yang, and A. H. MacDonald, Nanotech. **23**, 052001 (2012).
 - ¹² I. L. Aleiner, D. E. Kharzeev and A. M. Tsvelik, Phys. Rev. B **76**, 195415 (2007).
 - ¹³ Y. Zhang, Z. Jiang, J.P. Small, M.S. Purewal, Y.-W. Tan, M. Fazlollahi, J.D. Chudow, J.A. Jaszczak, H.L. Stormer, and P. Kim, Phys. Rev. Lett. **96**, 136806 (2006).
 - ¹⁴ D. A. Abanin, K. S. Novoselov, U. Zeitler, P. A. Lee, A. K. Geim, and L. S. Levitov, Phys. Rev. Lett. **98**, 196806 (2007).
 - ¹⁵ Z. Jiang, Y. Zhang, H. L. Stormer, and P. Kim, Phys. Rev. Lett. **99**, 106802 (2007).
 - ¹⁶ J. G. Checkelsky, L. Li, and N. P. Ong, Phys. Rev. Lett. **100**, 206801 (2008);
 - ¹⁷ J. G. Checkelsky, L. Li, and N. P. Ong, Phys. Rev. B **79**, 115434 (2009).
 - ¹⁸ A. J. M. Giesbers, L. A. Ponomarenko, K. S. Novoselov, A. K. Geim, M. I. Katsnelson, J. C. Maan, and U. Zeitler, Phys. Rev. B **80**, 201403(R) (2009).
 - ¹⁹ X. Du, I. Skachko, F. Durr, A. Luican, and E. Y. Andrei, Nature, **462**, 192 (2009).
 - ²⁰ K. I. Bolotin, F. Ghahari, M. D. Shulman, H. L. Stormer, and P. Kim, Nature, **462**, 196 (2009).
 - ²¹ L. Zhang, Y. Zhang, M. Khodas, T. Valla, I. A. Zaliznyak, Phys. Rev. Lett. **105**, 046804 (2010).
 - ²² Y. Zhao, P. Cadden-Zimansky, F. Ghahari, and P. Kim, Phys. Rev. Lett. **108**, 106804 (2012).
 - ²³ A. F. Young, C. R. Dean, L. Wang, H. Ren, P. Cadden-Zimansky, K. Watanabe, T. Taniguchi, J. Hone, K. L. Shepard, and P. Kim, Nature Phys. **8**, 550 (2012)
 - ²⁴ A. F. Young, J. D. Sanchez-Yamagishi, B. Hunt, S. H. Choi, K. Watanabe, T. Taniguchi, R. C. Ashoori, P. Jarillo-Herrero, Nature **505**, 528 (2014).
 - ²⁵ F. Chiappini, S. Wiedmann, K. S. Novoselov, A. Mishchenko, A. K. Geim, J. C. Maan, and U. Zeitler, Phys. Rev. B **92**, 201412 (R) (2015).
 - ²⁶ K. Nomura and A. H. MacDonald, Phys. Rev. Lett. **96**, 256602 (2006); K. Yang, S. Das Sarma, and A. H. MacDonald, Phys. Rev. B **74**, 075423 (2006).
 - ²⁷ D. A. Abanin, P. A. Lee, and L. S. Levitov, Phys. Rev. Lett. **96**, 176803 (2006); Solid State Commun. **143**, 77 (2007).
 - ²⁸ M. O. Goerbig, R. Moessner, and B. Douçot, Phys. Rev. B **74**, 161407(R) (2006).
 - ²⁹ J. Alicea and M. P. A. Fisher, Phys. Rev. B **74**, 075422 (2006).
 - ³⁰ L. Sheng, D. N. Sheng, F. D. M. Haldane, and L. Balents, Phys. Rev. Lett. **99**, 196802 (2007).
 - ³¹ G. W. Semenoff and F. Zhou, JHEP **1107**, 037 (2011).
 - ³² M. M. Fogler and B. I. Shklovskii, Phys. Rev. B **52**, 17366 (1995).
 - ³³ V. P. Gusynin, V. A. Miransky and I. A. Shovkovy, Phys. Rev. Lett. **73**, 3499 (1994) [Phys. Rev. Lett. **76**, 1005 (1996)].
 - ³⁴ I. A. Shovkovy, Lect. Notes Phys. **871**, 13 (2013).
 - ³⁵ V. A. Miransky and I. A. Shovkovy, Phys. Rept. **576**, 1 (2015).
 - ³⁶ D. V. Khveshchenko, Phys. Rev. Lett. **87**, 206401 (2001); Phys. Rev. Lett. **87**, 246802 (2001).
 - ³⁷ V. P. Gusynin, V. A. Miransky, S. G. Sharapov and I. A. Shovkovy, Phys. Rev. B **74**, 195429 (2006).
 - ³⁸ J.-N. Fuchs and P. Lederer, Phys. Rev. Lett. **98**, 016803 (2007).
 - ³⁹ M. Ezawa, J. Phys. Soc. Jpn. **76**, 094701 (2007); Physica E **40**, 269 (2007).
 - ⁴⁰ E. V. Gorbar, V. P. Gusynin, and V. A. Miransky Low Temp. Phys. **34**, 790 (2008).
 - ⁴¹ E. V. Gorbar, V. P. Gusynin, V. A. Miransky and I. A. Shovkovy, Phys. Rev. B **78**, 085437 (2008).
 - ⁴² I. F. Herbut, Phys. Rev. Lett. **97**, 146401 (2006); Phys. Rev. B **75**, 165411 (2007); Phys. Rev. B **76**, 085432 (2007).
 - ⁴³ I. F. Herbut, V. Juričić, and B. Roy, Phys. Rev. B **79**, 085116 (2009).
 - ⁴⁴ M. Kharitonov, Phys. Rev. B **85**, 155439 (2012).
 - ⁴⁵ J. Jung and A. H. MacDonald, Phys. Rev. B **80**, 235417 (2009).
 - ⁴⁶ K. Nomura, S. Ryu, D.-H. Lee, Phys. Rev. Lett. **103**, 216801 (2009).
 - ⁴⁷ B. Roy, M. P. Kennett, and S. Das Sarma, Phys. Rev. B **90**, 201409(R) (2014).
 - ⁴⁸ E. V. Gorbar, V. P. Gusynin, V. A. Miransky, and I. A. Shovkovy, Phys. Scripta T **146**, 014018 (2012).
 - ⁴⁹ P. K. Pyatkovskiy and V. P. Gusynin, Phys. Rev. B **83**, 075422 (2011).

- ⁵⁰ E. V. Gorbar, V. P. Gusynin, V. A. Miransky, and I. A. Shovkovy, Phys. Rev. B **85**, 235460 (2012).
- ⁵¹ M. L. Sadowski, G. Martinez, M. Potemski, C. Berger, and W.A. de Heer, Phys. Rev. Lett. **97**, 266405 (2006).
- ⁵² Z. Jiang, E. A. Henriksen, L. C. Tung, Y.-J. Wang, M. E. Schwartz, M. Y. Han, P. Kim, and H. L. Stormer, Phys. Rev. Lett. **98**, 197403 (2007).
- ⁵³ M. Orlita and M. Potemski, Semicond. Sci. Technol. **25**, 063001 (2010).
- ⁵⁴ A. Iyengar, J. Wang, H. A. Fertig, and L. Brey, Phys. Rev. B **75**, 125430 (2007).